The LINNEAN SOCIETY of London BIOLOGICAL Journal of the Linnean Society

Biological Journal of the Linnean Society, 2016, **117**, 686–704.

To what extent do new fossil discoveries change our understanding of clade evolution? A cautionary tale from burying beetles (Coleoptera: *Nicrophorus*)

EMMANUEL F. A. TOUSSAINT[1*,†] and FABIEN L. CONDAMINE[2†]

[1]*Department of Ecology & Evolutionary Biology & Division of Entomology, Biodiversity Institute, University of Kansas, Lawrence, KS, 66045, USA*
[2]*Department of Biological Sciences, University of Alberta, Edmonton, AB, T6G 2E9, Canada*

Received 6 July 2015; revised 24 September 2015; accepted for publication 25 September 2015

Divergence time estimates derived from phylogenies are crucial to infer historical biogeography and diversification dynamics. Yet, the impact of fossil record incompleteness on macroevolutionary reconstructions remains equivocal. Here, we investigate to what extent gaps in the fossil record can impinge downstream evolutionary inferences in the beetle family Silphidae. Recent discoveries have pushed back the fossil record of this group from the Eocene into the Jurassic. We estimated the divergence times of the family using both its currently understood fossil record and the fossil record known prior to these recent discoveries. All fossil calibrations were informed with different parametric distributions to investigate the weight of priors on posterior age estimates. Based on time-calibrated trees, we assessed the impact of fossil calibrations on the inference of ancestral ranges and diversification rate dynamics in the genus *Nicrophorus*. Depending upon the selected sets of fossil constraints, the age discrepancies had a major impact on the macroevolutionary inferences: the biogeographic extrapolations relative to paleogeography are markedly contrasting, and the calculated rates at which species form or go extinct (and when they varied) are strikingly different. We show that soft prior distributions do not necessarily alleviate such shortcomings therefore preventing the inference of reliable macroevolutionary patterns in groups presenting a taphonomic bias in their fossil record. *Biological Journal of the Linnean Society*, 2016, **117**, 686–704.

ADDITIONAL KEYWORDS: biogeography – diversification – extinction – fossils – molecular dating – Silphidae.

INTRODUCTION

Our understanding of the tempo and mode of clade evolution depends upon phylogenetic and dating reconstructions (Smith & Peterson, 2002; Hedges & Kumar, 2009; Hedges *et al.*, 2015) but also upon the fossil record (Alroy, 2010; Smith & Marcot, 2015). Calibrating molecular clocks is a crucial step to date lineage diversification and understand biodiversity assembly over time and space (Donoghue & Benton, 2007; Ho & Duchêne, 2014; Bell, 2015). In the last decade, increasingly sophisticated methods have been developed to handle large molecular datasets and to model rate variation among lineages (e.g. Drummond *et al.*, 2012; Ronquist *et al.*, 2012; reviewed in Rutschmann, 2006; Ho & Duchêne, 2014; Bell, 2015). Yet, proper calibration of molecular clocks to obtain absolute divergence times can be challenging (e.g. Dornburg *et al.*, 2011; Lukoschek, Scott Keogh & Avise, 2012; Warnock *et al.*, 2015). Hence, identifying and dealing with sources of error in calibrations is fundamental in the dating process (Ho & Phillips, 2009; Inoue, Donoghue & Yang, 2010; Parham *et al.*, 2012).

Traditionally, external information is needed to enforce age constraints in a phylogenetic tree (Donoghue & Benton, 2007; Ho & Phillips, 2009). Such calibrations are often based on biogeographic events (e.g. island formation or continental breakup; Kodandaramaiah, 2011) or fossil evidence that respectively provides maximum or minimum ages for a focal

*Corresponding author. E-mail: toussaint@ku.edu
†These authors contributed equally to this work.

clade (Donoghue & Benton, 2007; Ho & Phillips, 2009; Parham *et al.*, 2012). When relying on the fossil record, dating analyses are sensitive to the incompleteness of the fossil record, referred to as the taphonomic bias (e.g. Smith & Peterson, 2002; Dornburg *et al.*, 2011). To accommodate the biases imposed by the fossil record, several methods implementing relaxed-clock models have been introduced (Yang & Rannala, 2006; Sanders & Lee, 2007; reviewed in Ho & Phillips, 2009). To mitigate the impact of potential errors in calibration choice, Yang & Rannala (2006) introduced the concept of soft bounds where a nonzero probability is assigned to ages found beyond specified bounds. The most recent methods, as implemented for instance in BEAST (Drummond *et al.*, 2006, 2012) and MrBayes (Ronquist *et al.*, 2012), allow the specification of distribution priors on targeted nodes in the tree (Sytsma, Spalink & Berger, 2014). The use of parametric distributions offers a greater flexibility and can theoretically provide a means to take into account the taphonomic bias (Dornburg *et al.*, 2011).

When it comes to dating a phylogenetic tree, evolutionary biologists may wonder to what extent an incomplete fossil record can render divergence time estimation spurious. Indeed, the fossil record is susceptible to only reflect tracks of a lineage evolution biased towards the Present (Lu, Yogo & Marshall, 2006). The probability of fossil preservation increases toward the Present, and large gaps often artificially truncate the distribution of lineages at deeper time scales (e.g. Romer's gap, Garrouste *et al.*, 2012). Numerous taxonomic groups have a fossil record highly concentrated into Cenozoic deposits (e.g. butterfly and moths, Sohn, Labandeira & Davis, 2015), which in turn might suggest a Cenozoic origin for many clades. As a result, macroevolutionary inferences may be severely biased by a truncated fossil record (Dornburg *et al.*, 2011). Recently, numerous fossil discoveries from Jurassic and Cretaceous beds in China, have pushed back in time the origin of well documented clades such as non-avian dinosaurs (e.g. Zhang *et al.*, 2008; Choiniere *et al.*, 2010; Xu, Zheng & You, 2010; Xu *et al.*, 2015), mammals (e.g. Yuan *et al.*, 2013; Zhou *et al.*, 2013; Meng *et al.*, 2015), or birds (e.g. Hu *et al.*, 2009; Xu *et al.*, 2011). Among invertebrates, several fossil discoveries were also made in the past decade (e.g. Kirejtshuk *et al.*, 2010) but probably with lesser scientific impacts than in vertebrate groups (but see Garrouste *et al.*, 2012; Huang *et al.*, 2012, 2013; Nel *et al.*, 2013). Among the most astonishing fossils to be discovered recently is the golden orb-weaver spider from the Middle Jurassic of China (Selden, Shih & Ren, 2011). This new fossil pushed back the origin of the cosmopolitan genus *Nephila* by 130 Myr, from the Miocene (Su *et al.*, 2011) to the Jurassic. These discoveries were paramount to our understanding of temporal origins, but also tempo and modes of diversification, character evolution or biogeographic histories (e.g. Luo, 2007; Lee *et al.*, 2014; Brusatte *et al.*, 2015). Yet, the extent to what taphonomic biases (incomplete fossil record) hamper macroevolutionary discussions drawn from phylogenetic studies has been largely overlooked.

Invertebrate clades are generally much older than vertebrate clades of the same taxonomic rank and thus provide a unique window to apprehend much older macroevolutionary patterns and processes (Hedges *et al.*, 2015). An important recent fossil discovery for insects was made in carrion beetles (Coleoptera: Silphidae) (Cai *et al.*, 2014). The family Silphidae notably comprises the subfamily Nicrophorinae including the charismatic *Nicrophorus* burying beetles (68 described species), as well as the two other genera *Ptomascopus* (four species) and *Eonecrophorus* (one species) (Sikes, Madge & Newton, 2002; Sikes, Madge & Trumbo, 2006). The existence of Silphidae in the Jurassic has already been invoked (e.g. Beutel & Leschen, 2005), but in most cases these fossils were likely poor taxonomic assignations, partly due to the fact that the contours of the family were blurry (Grebennikov & Newton, 2012). Therefore, silphids were long thought to have originated and diversified in the Cenozoic (Flach, 1890; Sikes & Venables, 2013). Until recently, their fossil record traced back to the late Eocene (Florissant bed, USA). Recent discoveries from China fossil rock beds in the Yixian formation (Early Cretaceous, Aptian-Berrenian, 121.0–125.0 Mya, Chang *et al.*, 2009) and in the Daohugou beds (Middle Jurassic, Oxfordian, 157.3–163.5 Mya, Wang *et al.*, 2005) as well as Myanmar amber fossils (Late Cretaceous, Cenomanian, 93.9–100.5 Mya) changed substantially our knowledge of the fossil record in this family (Grebennikov & Newton, 2012; Cai *et al.*, 2014). These newly discovered fossils extend the earliest records of carrion beetles (Silphidae) by about 130 Myr, the one of the subfamily Nicrophorinae by about 100 Myr, and the one of burying beetles (*Nicrophorus*) by about 90 Myr (Cai *et al.*, 2014). This family therefore represents an ideal candidate to investigate the impact of the taphonomic bias on molecular dating studies, a scenario that can be more common than previously thought (Gao & Shubin, 2003, 2012; Dornburg *et al.*, 2011; Selden *et al.*, 2011).

Here, we use a comprehensive burying beetle molecular dataset (Sikes & Venables, 2013) to: (1) test to what extent Bayesian relaxed-clock approaches allow us to overcome the taphonomic bias using multiple prior distributions for modelling fossil calibrations, and (2) assess the possible differences in macroevolutionary patterns by inferring

biogeographic histories and estimating rates of diversification within *Nicrophorus*. Our study recovers markedly different age estimates between the two calibration sets used. The flexibility of molecular clock calibration priors did not overcome the fossil record bias. As a result we infer two distinct evolutionary histories for *Nicrophorus* burying beetles depending upon the calibrations set considered.

METHODS

Taxon sampling and molecular dataset

The molecular dataset was retrieved from Sikes & Venables (2013). It comprises 63 specimens including 54 out of the 68 valid extant species of the genus *Nicrophorus* (i.e. 80% of its total diversity) as well as one species of the genus *Ptomascopus* out of the four valid extant species (Sikes *et al.*, 2002, 2006). It also included four species of the subfamily Silphinae as well as a more distant outgroup, the rove beetle species *Aleochara heeri* (Staphylinidae). The molecular dataset consisted of three mitochondrial gene fragments, cytochrome *c* oxidase subunit I (COI, 1428 nucleotides), tRNA (85 nucleotides) and cytochrome *c* oxidase subunit II (COII, 687 nucleotides), and two nuclear gene fragments, the 28S ribosomal RNA segment D2 (28S, 908 nucleotides), and the protein coding gene carbamoyl-phosphate synthase (CAD, 792 nucleotides). In total, the dataset contained 3971 aligned nucleotides.

Divergence time estimations

Estimations of divergence times were inferred with Bayesian inference as implemented in BEAST 1.8.2 (Drummond *et al.*, 2012) based on the molecular phylogeny retrieved from Sikes & Venables (2013). Where relevant, we mention the methodological differences between the analyses conducted by Sikes & Venables (2013) and our analyses. We ran a PartitionFinder v.1.1.1 (Lanfear *et al.*, 2012) analysis to select the best-fitting models of substitution using the '*greedy*' algorithm, the *'beast'* set of models and the corrected Akaike Information Criterion (AICc) to compare the fit of the different models. We tested the hypothesis of molecular clock using Paup* (Swofford, 2003), and since it was significantly rejected ($P < 0.001$), we used a Bayesian relaxed-clock allowing rate variation among lineages as implemented in BEAST (Drummond *et al.*, 2006, 2012).

Bayesian relaxed-clock settings

We implemented partitioned relaxed-clock models with an uncorrelated lognormal clock model that assumes an underlying lognormal distribution (UCLD) of the evolutionary rates (Drummond *et al.*, 2006). We specified a clock model for each of the partition recovered in PartitionFinder except for the mitochondrial partitions for which a unique model was specified. Using BEAUti 1.8.2, we set the following priors: a *birth–death process* (Gernhard, 2008) as branching process prior (Sikes & Venables (2013) set the Yule model), shaped by a uniform prior between 0 and 10 with a starting value at 0.1 for the *birth–death mean growth rate*, and a uniform prior between 0 and 1 with a starting value at 0.5 for the *birth-death relative death rate*. We used an exponential prior with mean one-third on the standard deviation of the UCLD model, and a uniform prior between 0 and 1 on the mean of the UCLD model. The tree topology was fixed to match that of Sikes & Venables (2013). The Markov chain Monte Carlo (MCMC) analyses were run for 100 million generations and sampled every 2000 generations, resulting in 50 000 trees in the posterior distribution; we discarded the first 12 500 trees as burn-in (25%).

Analysis and convergence

Tracer was used to graphically assess the convergence of runs (Rambaut *et al.*, 2015), after checking the log-likelihood curves (stationarity of the MCMC) and the different runs merged using LogCombiner 1.8.2 (Drummond *et al.*, 2012). We also checked the effective sample size (ESS) for all parameters, for which we consider that ESS values above 200 indicate good convergence. For each analysis, we conducted two independent runs to ensure convergence of the MCMC. Post burn-in trees from the two distinct runs were further combined to build the maximum clade credibility (MCC) tree, median ages and their 95% highest posterior density (HPD) were generated afterwards under TreeAnnotator 1.8.2 (Drummond *et al.*, 2012).

Fossil calibrations and prior distributions

Divergence times were inferred using two distinct calibration sets based on an extensive survey of the carrion-beetle fossil record literature: (1) a first calibration set using fossil information available prior to the discovery of Mesozoic fossils from China and Myanmar (Cai *et al.*, 2014), and (2) a second calibration set using all fossil information in the carrion-beetle fossil record (Fig. 1). The extant fossil record of carrion beetles encompasses the past 165 Myr and until the study of Cai *et al.* (2014), only a few valid fossils were known for this group. In a conservative manner, we systematically selected the oldest known fossil of a crown group to calibrate the corresponding node in the dating analyses. The absolute fossil ages we used are derived from the latest geological timescale.

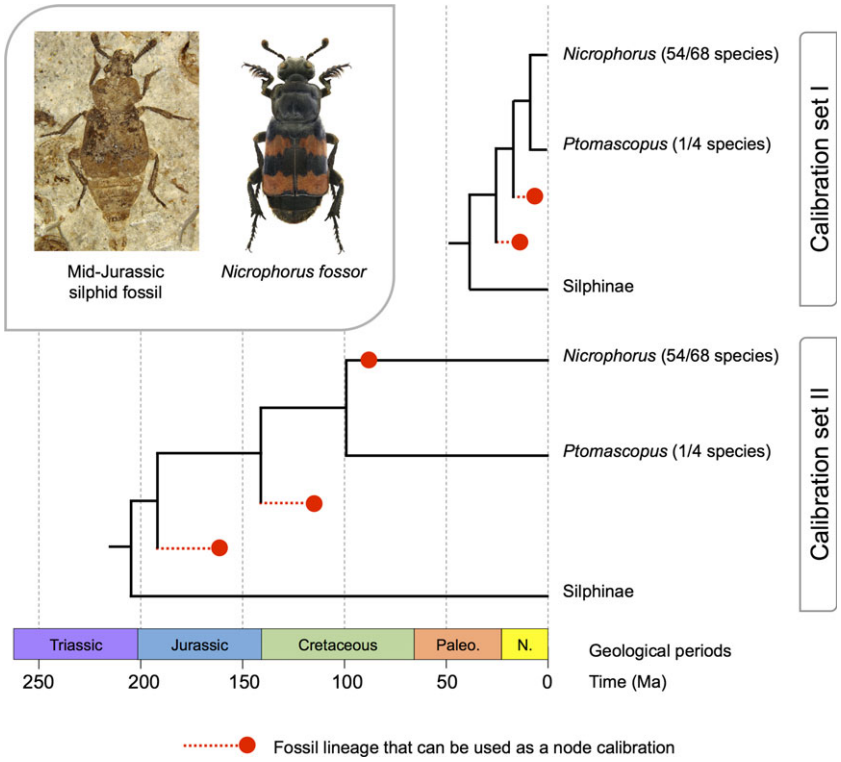

Figure 1. Schematic representation of the two calibration sets used in this study to date the origin of burying beetles. The first calibration set uses the Cenozoic fossils, which were the most ancient fossils known for the group prior to the discoveries in China. The second calibration set employs the Mesozoic fossils recently discovered in the Daohugou beds, China (Cai *et al.*, 2014). Illustrated are an extinct and an extant silphid species, showing how the morphological features are preserved and thus allow a safe assignation of fossil lineages as node calibrations. Paleo., Paleogene; and N., Neogene. Pictures from © Wikimedia Commons.

One of the aims of this study was to test whether modern dating approaches can alleviate the taphonomic bias of the fossil record. Therefore, we independently used exponential, lognormal and uniform distributions as priors to calibrate the nodes of the topology (where Sikes & Venables (2013) set a normal prior for each fossil calibration). The exponential distribution allows modelling with two parameters a long tail of diminishing probability with the maximal probability being located at the minimum bound of the specified interval. On the other hand, the lognormal distribution requires three parameters to assign a maximum probability to a different point than the minimum bound. Finally, the uniform distribution sets hard minimum and maximum ages with equal probability along the distribution.

The prior parameters (Fig. S1) were selected such that 95% of the distribution spanned an interval respectively starting from the lower bound of the fossil age and ending at 300 Mya, the approximate age of the order Coleoptera as estimated from a large-scale study using multiple fossil calibrations across the insect tree of life (Rainford *et al.*, 2014) and from the entire fossil record (Smith & Marcot, 2015).

First calibration set

We relied on the oldest fossils of Silphidae and Nicrophorinae prior to the publication of Cai *et al.* (2014). We first used †*Necrodes primaevus* Beutenmüller and Cockerell 1908, found in shales of the Florissant formation (Colorado, USA) and dated from the late Eocene (Priabonian, ~ 33.9–37.8 Mya), which is the oldest silphid fossil anterior to the publication of Cai *et al.* (2014). †*Silpha beutenmulleri* Wickham 1914, is also believed to be a silphid fossil from the same formation although it consists of a unique elytra. These two fossils are recognized as part of the family Silphidae without ambiguity but their classification among the different genera is not as clear and as a result we used these fossils to calibrate the crown of the family Silphidae rather than a more derived node. Additional fossils described almost a century ago have been considered and then rejected as possible valid fossils because they lack key morphological features of the family (e.g. clubbed

antennae, large mesoscutellum, truncate elytra, well separated mesocoxae) (Grebennikov & Newton, 2012). Accordingly, †*Eosilphites decoratus* (Germany, Eocene, Lutetian, ~ 41.2–47.8 Mya), †*Sinosilphia punctata* (China, Early Cretaceous, Aptian, ~ 113.0–125.0 Mya) or †*Prosilpha nigrita* (China, Early Cretaceous, Barremian, ~ 125–129.4 Mya) were ruled out and transferred to the Agyrtidae (Newton, 1997). Second, we used the two fossils of Nicrophorinae, namely †*Palaeosilpha fraasii* Flach, 1890; and †*Ptomascopus aveyronensis* Flach, 1890, found in a lacustrine phosphorite strata in Caylux (France) that are dated from the late Oligocene (Chattian, ~ 23.03–28.1 Mya). These two fossils are unequivocally placed in the subfamily Nicrophorinae (Newton & Cai pers. comm.) and were therefore used to calibrate the crown of this group.

Second calibration set

We used the updated fossil record from Cai *et al.* (2014) to calibrate internal nodes of the topology. Thanks to these new discoveries, we were able to place minimum age constraints on the following nodes: Silphidae (China, Middle Jurassic, Oxfordian, Daohugou beds, ~ 157.3–163.5 Mya, Wang *et al.*, 2005), Nicrophorinae (China, Early Cretaceous, Aptian-Barremian, Yixian formation, ~ 121.0–125.0 Mya, Chang *et al.*, 2009) and *Nicrophorus* (Myanmar, Late Cretaceous, Cenomanian, ~ 93.9–100.5 Mya).

Ancestral area reconstructions

The chronograms derived from the analyses using exponential priors were used. We selected these chronograms because all analyses yielded comparable age estimates (see Results) and because this distribution is usually preferred over the lognormal one that has one more parameter for the mode of its probability distribution (Ho & Phillips, 2009).

We first assessed the impact of fossil record on biogeographic inferences using the two MCC trees (one for each calibration set) obtained in BEAST with outgroups removed. Previously, Sikes & Venables (2013) inferred the biogeographic history using the asymmetrical 2-parameter Markov k-state model with user fixed rates set to equal on a binary dataset with the character states 'Old World' and 'New World'. Here we use the model DEC (Dispersal-Extinction-Cladogenesis) implemented in the program Lagrange (Ree & Smith, 2008) to infer the biogeographical history of the genus *Nicrophorus* across its entire range of distribution. Using tectonic reconstructions (e.g. Blakey, 2008; Seton *et al.*, 2012), we divided the distributional range of *Nicrophorus* species in six areas: (N) Nearctic, (T) Neotropics, (W) Western Palearctic, (E) Eastern Palearctic, (O) Oriental, and (A) Australasia. Distributional data were compiled from the literature (Sikes *et al.*, 2002, 2006).

We define and use a time-stratified model that will also be more sensitive to dating analyses. The adjacency matrix was designed whilst taking into account the geological history and the biological plausibility of combined areas (Blakey, 2008; Seton *et al.*, 2012). The dispersal rate values (dr) were calculated using the following rules: the dispersal rate between adjacent areas was not penalized (dr = 1.0), the dispersal rate between areas separated by a small water barrier was slightly penalized (dr = 0.75), the dispersal rate between areas separated by another area was moderately penalized (dr = 0.50), and the dispersal rate between areas separated by a large water barrier was strongly penalized (dr = 0.25). The final dispersal rate matrices between all possible area combinations were calculated following these rules and taking into account multiple barriers and landmass discontinuities throughout the timeframe of the group's evolution (Table S1; Blakey, 2008; Seton *et al.*, 2012). We always preferred the shortest path between two areas to calculate the dispersal rate values. In case of a dispersal rate value becoming zero as a result of several barriers and/or landmass discontinuities, we chose in a conservative manner to use a dr = 0.05 in order to take into consideration unlikely long-dispersal events (Table S1).

Three models were used: (1) M0, in which all area combinations are allowed and no dispersal rate constraints are imposed; (2) M1, in which the area combinations are restricted by the adjacency matrix but without dispersal rate constraints; and (3) M2, in which the area combinations are restricted by the adjacency matrix and dispersal rates constrained to reflect the geological configuration. In these models, we discarded ranges larger than four areas in size that were not subsets of observed species ranges (*Nicrophorus investigator* has the largest range with four areas) and also because all four regions were never connected during the evolution of the group. A model-testing procedure was adopted to optimize the ancestral range at the root. A significant ancestral area was selected when we found a difference of 2-log units in the log-likelihoods between two areas or combination of areas.

Diversification analyses

We then assessed the impact of fossil record on the macroevolutionary inferences using various models of diversification. We used the same trees as for the biogeographic analyses.

Time-dependent diversification

We assessed whether diversification rates remained constant during the evolutionary history of the genus

Nicrophorus. In particular, we tested whether periods of extinction might be recovered with birth-death models. The TreePar R-package (Stadler, 2011) was used to calculate speciation and extinction rates through time. This method relaxes the assumption of constant rates by allowing rates to change at specific points in time. We employed the '*bd.shifts.optim*' function that allows the estimation of discrete changes in speciation and extinction rates and mass extinction events in under-sampled phylogenies (Stadler, 2011). At each time t, the rates are allowed to change and the group may undergo a shift in diversification. TreePar analyses were run with the two maximum credibility trees of the BEAST analyses (one for each calibration set) as well as with 100 posterior trees randomly collected from the BEAST analysis of the second calibration set. The analyses were conducted with the following settings: start = just after the most recent divergence time (T. Stadler pers. comm.), end = crown age estimated by the dating analyses, grid = 0.1 Myr, and posdiv was set to FALSE to allow the diversification rate to be negative.

To complement the inferences made with TreePar, we used the Bayesian Analysis of Macroevolutionary Mixture (BAMM) to estimate speciation and extinction rates through time and among/within clades (Rabosky *et al.*, 2013; Rabosky, 2014). BAMM allows studying complex evolutionary processes on phylogenetic trees, potentially shaped by a heterogeneous mixture of distinct dynamics of speciation and extinction across clades (clades might have different rates). The method can automatically detect rate shifts without *a priori* hypotheses and sample distinct evolutionary dynamics that best explain the whole diversification dynamics. BAMM allows time-variable diversification rates, with the speciation rate varying exponentially through time while extinction is maintained constant (Rabosky, 2014). BAMM provides estimates of marginal probability of speciation and extinction rates at any point in time along any branch of the tree.

We ran BAMM analyses using the C++ command line program, setting four reversible-jump MCMC (Huelsenbeck, Larget & Alfaro, 2004) running for 10 million generations and sampled every 10 000 generations. A compound Poisson process is implemented in BAMM for the prior probability of a rate shift along any branch. We used a prior value of 1.0 implying a null hypothesis of no rate shift across the phylogeny, as recommended by Rabosky (2014) for a phylogeny with < 500 species. We accounted for incomplete taxon sampling using the implemented analytical correction, with a sampling fraction set to 0.794 (i.e. 54 species out of the 68 described species). We performed four independent runs (with a burn-in of 10%) using different seeds, and we used ESS to assess the convergence of the runs, considering values above 200 indicating good convergence. We analyzed the BAMM output using the R-package BAMMtools (Rabosky *et al.*, 2014). Marginal probabilities of the number of evolutionary regimes were computed and the models were compared with Bayes factors (Kass & Raftery, 1995). The posterior distribution was also used to estimate the best configuration and the 95% credible set diversification models were compared using Bayes factors.

Diversity-dependent diversification

We investigated whether lineages diversified rapidly in their early stage, and secondly reached an equilibrium meaning that diversity is saturated at the Present as niches become occupied and diversification rates slowed down (McVay, Flores-Villela & Carstens, 2015; Peña *et al.*, 2015). We used the method of Etienne *et al.* (2012) to explore the effect of diversity on speciation and extinction rates. The function '*dd_ML*' was used to fit five models: (1) speciation declines linearly with diversity and no extinction (DDL), (2) speciation declines linearly with diversity and extinction (DDL+E), (3) speciation declines exponentially with diversity and extinction (DDX+E), (4) extinction increases linearly with diversity (DD+EL), and (5) extinction increases exponentially with diversity (DD+EX). The initial carrying capacity was set to the current species diversity (which assumes that all species have been described), and the final carrying capacity (noted as K) was estimated according to the models and parameters.

RESULTS

Estimates of divergence times

All BEAST analyses converged well for both calibration sets and for each prior distribution on the fossil calibrations as indicated by ESS above 200 for all parameters. Results of the dating analyses are presented in Figs 2 and 3 (see Fig. S2 for the chronograms with 95% HPD at each node). All analyses based on a similar calibration set yielded highly comparable divergence time estimates (Fig. 2, Fig. S2). The analyses based on the exponential and lognormal prior distributions resulted in almost identical credibility intervals whereas the ones based on the uniform prior distributions resulted in broader credibility intervals, but with similar median ages. In all cases, the dating analyses based on the first set of calibrations yielded much younger estimates than the one resulting from the second set of calibrations (Fig. 2). The credibility intervals of both calibration sets for a given analysis were never overlapping except at derived nodes. In summary, the first

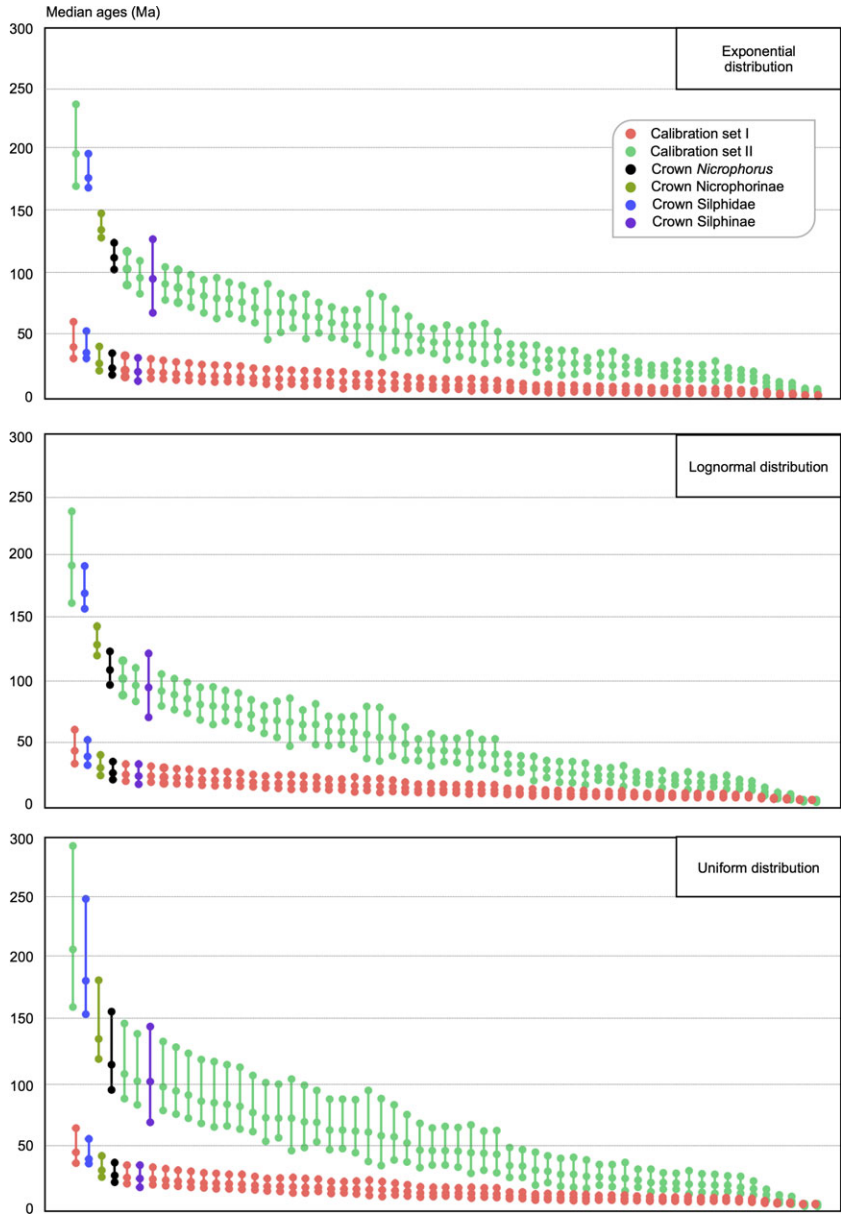

Figure 2. Differences of divergence times estimates for both calibration sets. The graphic highlights how the fossil record impacts the molecular estimates obtained with the BEAST dating analyses. In the first calibration set, most of the events occurred in the Neogene, whereas in the second set most of the events happened in the Cretaceous and Paleogene. Four important nodes (origin of major clades) are represented, which shows that the 95% HPD did not overlap between the two calibration sets.

calibration set finds an origin of these two lineages respectively in the middle Eocene (44.4 Mya, 95% HPD 34.1–67.4 Mya) and in the late Oligocene (25.3 Mya, 95% HPD 19.2–39.0 Mya) (Fig. 3). Conversely, the second set of calibrations recovers an origin of silphids in the Early Jurassic (192.3 Mya, 95% HPD 166.2–232.3 Mya) and of the genus *Nicrophorus* at the end of the Early Cretaceous (108.5 Mya, 95% HPD 99.0–120.7 Mya). In comparison, Sikes & Venables (2013) found the origin of Silphidae at 175.7 Mya (95% HPD 164.1–186.3 Mya), of Nicrophorinae at 133.4 Mya (95% HPD 123.9–144.4 Mya), and of *Nicrophorus* at 113.2 (95% HPD 98.8–126.9 Mya).

Biogeographic analyses

All Lagrange analyses (for the three models M0, M1, and M2) provided similar biogeographic inferences and

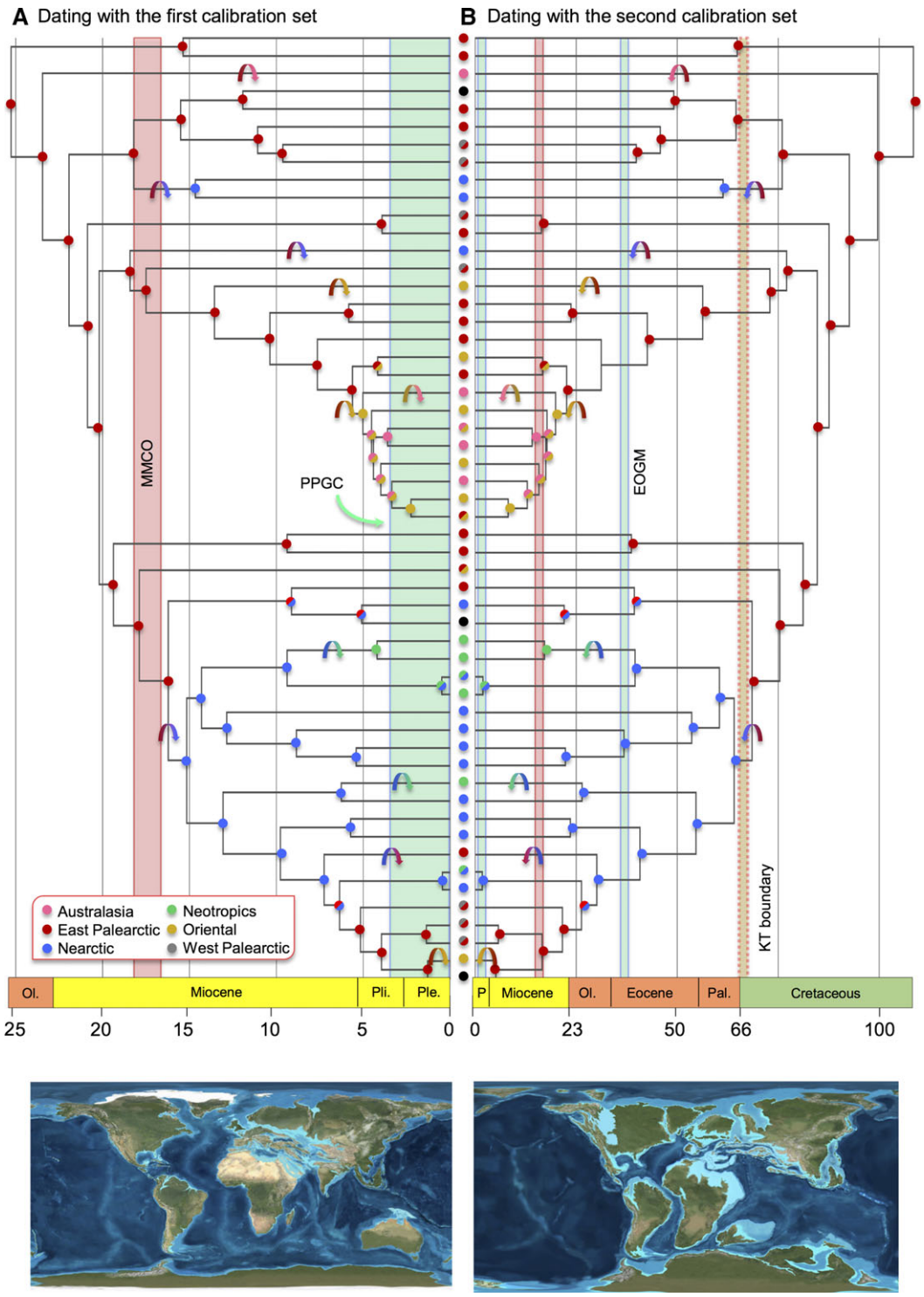

Figure 3. Historical biogeography of burying beetles as inferred based on the two calibration set chronograms. (A) Maximum clade credibility tree with median ages using the first calibration set. (B) Maximum clade credibility tree with median ages using the second calibration set. For each timetree, estimates of the likeliest ancestral biogeographic ranges (inferred with Lagrange and the DEC model) are indicated at each node by colored circles correspond to the inset. KT boundary, Cretaceous-Paleogene extinction; EOGM, early Oligocene glacial maximum; MMCO, middle Miocene climatic optimum; PPGC, Plio-Pleistocene glaciation cycles. Absolute ages are in million years, and the paleo-maps are from Blakey (2008).

Table 1. Results of the biogeographical analyses made with Lagrange and the DEC model

	Set of calibrations 1			Set of calibrations 2		
Root model	M0	M1	M2	M0	M1	M2
Australasia (A)	−150.8	−143.8	−141.6	−150.6	−143.4	−142.0
East Palearctic (E)	**−143.9**	**−132.1**	**−130.0**	**−143.9**	**−132.0**	**−131.0**
Nearctic (N)	−151.8	−140.7	−138.4	−151.6	−140.4	−139.4
Neotropics (T)	−154.7	−151.0	−149.0	−154.4	−150.4	−150.1
Oriental (O)	−154.5	−137.2	−134.9	−154.2	−137.0	−135.4
West Palearctic (W)	−154.3	−142.1	−139.8	−154.0	−141.8	−141.0

For each set of calibrations, we report the log-likelihood value obtained for the biogeographical analyses optimized at the root and for each component area in the models. Three models were applied: M0, all area combinations allowed + no dispersal rate constraints; M1, area combinations restricted by an adjacency matrix + no dispersal rate constraints; M2, area combinations restricted by an adjacency matrix + dispersal rates constrained to reflect paleoreconstructions. All analyses supported the East Palearctic as the ancestral area. Bold values depict the best-fit diversification model.

ancestral range at the root (Table 1). For both timetrees, the root optimizations significantly supported East Palearctic as the most likely ancestral area (Table 1). Results of the biogeographic inferences are presented in Figure 3. First, all analyses recovered two early dispersal events toward the Nearctic region but at different times. In the first set of calibrations, these two dispersal events occur just after the mid-Miocene climatic optimum (MMCO, Zachos *et al.*, 2001), whereas in the second set of calibrations these events happen after the Cretaceous-Paleogene (K-Pg) mass extinction (Fig. 3). Second, there was also an early dispersal towards Australasia although the evolutionary sequence is equivocal because this lineage evolved in a unique extant species. Third, we recovered three later main dispersal events in the evolution of *Nicrophorus* that took place broadly at the same time: (1) the Neotropics were colonized out of the Nearctic region during the past 5 Myr in the first set of calibrations and during the early Miocene in the second one; (2) the colonization of the Oriental region and Australasia from East Palearctic is found with an evolutionary sequence broadly matching the respective timings of the Neotropics colonization in both reconstructions. Finally, we unveil a back colonization from the Nearctic region towards the East Palearctic again during the same timeframe with subsequent colonization of the Oriental region. Overall we highlight a dynamic biogeographic pattern with a surprisingly similar pattern between both sets of calibration. If the reconstructed ancestral areas at each node are matching, the evolutionary sequence of the processes that led to this biogeographical pattern are markedly different.

Diversification analyses

The TreePar analyses rejected the hypothesis of a rate-constant diversification within *Nicrophorus* burying beetles for both timetrees (Table 2, Table S2). However the two timetrees significantly differ in their pattern of diversification: a model with one shift of diversification better explained the timetree obtained with the first calibration set, while a model with three shifts better explained the timetree obtained with the second calibration set (at P (LRT) < 0.05, Table 2). Besides, both timetrees significantly differ in the time when diversification changed: the timetree with the first calibration set showed a shift in the late Pliocene (≈3.3 Mya), whereas the timetree with the second calibration set showed a first shift in the middle Miocene (≈15.8 Mya), with a second and third in the late Eocene (≈37.7 Mya and 40.9 Mya) (Fig. 4). The timetree with the first calibration set showed a decrease of diversification through time, with higher rates of diversification at the origin of the clade and lower rates towards the Present, while the turnover (ratio of extinction over speciation) increased over time (Table 2a, Fig. 4). The timetree with the second calibration set indicated a more dynamic pattern that is explained by a medium initial diversification rate until a burst of diversification occurred after the first time shift, 41 Mya. At the second shift, 38 Mya, the clade experienced a decline of diversity due to negative net diversification rate (Table 2b, Fig. 4). This decline of diversity is estimated to have lasted until the third shift at 16 Mya. After this time and onwards, a period of diversity recovery began for the clade (with positive net diversification rate again). The turnover increased over time, except in the last period of diversification (i.e. between Present and the first shift). We investigated the robustness of this result applying TreePar on 100 posterior trees, and found a very similar result: the best-fitting model has three shifts of diversification closely matching the shifts estimated with the

Table 2. Results of the time-dependent diversification analyses made with TreePar

Model	NP	logL	*P* (LRT)	r. 1	τ 1	s.t. 1	r. 2	τ 2	s.t. 2	r. 3	τ 3	s.t. 3	r. 4	τ 4	s.t. 4	r. 5	τ 5
(a) Timetree obtained with the first calibration set																	
No shift time	2	−138.057	Null model	0.1066	0	–	–	–	–	–	–	–	–	–	–	–	–
1 shift time	**5**	**−132.8028**	**0.0147**	**0.036**	**0.0371**	**3.267**	**0.1337**	**0**	–	–	–	–	–	–	–	–	–
2 shift times	8	−130.1778	0.1544	−0.2937	6.1148	3.267	1.00E-04	0.9998	13.067	0.2476	0.7977	–	–	–	–	–	–
3 shift times	11	−129.2369	0.3088	−0.4765	7.1816	3.267	0.0184	0.981	13.067	0.2773	0.8317	23.567	1.00E-04	0.7539	–	–	–
4 shift times	14	−127.9959	0.3826	−0.4057	6.701	3.267	0.0158	0.9795	13.067	0.2412	0.8328	23.367	2.6589	0.7848	23.567	1.00E-04	0.7942
(b) Timetree obtained with the second calibration set																	
No shift time	2	−212.4908	Null model	0.0255	0	–	–	–	–	–	–	–	–	–	–	–	–
1 shift time	5	−207.8389	0.0255	0.0109	0	15.76	0.032	0.0184	–	–	–	–	–	–	–	–	–
2 shift times	8	−204.1333	0.0599	0.0067	0.408	15.76	−0.0698	1.8849	37.66	0.0456	0.8046	–	–	–	–	–	–
3 shift times	**11**	**−201.3603**	**0.0437**	**0.001**	**0.9181**	**15.76**	**−0.0977**	**1.9919**	**37.66**	**0.2907**	**0.651**	**40.86**	**0.0578**	**0.5785**	–	–	–
4 shift times	14	−199.4811	0.0534	0.0012	0.9017	15.76	−0.0802	1.8962	36.86	−1.2902	2.654	37.66	0.6772	0.0209	40.86	0.0636	0

The model 'No shift time' is a constant-rate birth-death model, and is the null model to be compared to more complex models that include shifts of diversification. Abbreviations are as follows: NP, number of parameters; logL, log-likelihood; *P* (LRT), *P*-value for the likelihood ratio test; r. 1, net diversification rate 1 (from Present to the first shift time going backward); τ 1, turnover 1 (from Present to the first shift time going backward); and s.t. 1, shift time 1 (i.e. period when the diversification changed). Bold values depict the best-fit diversification model.

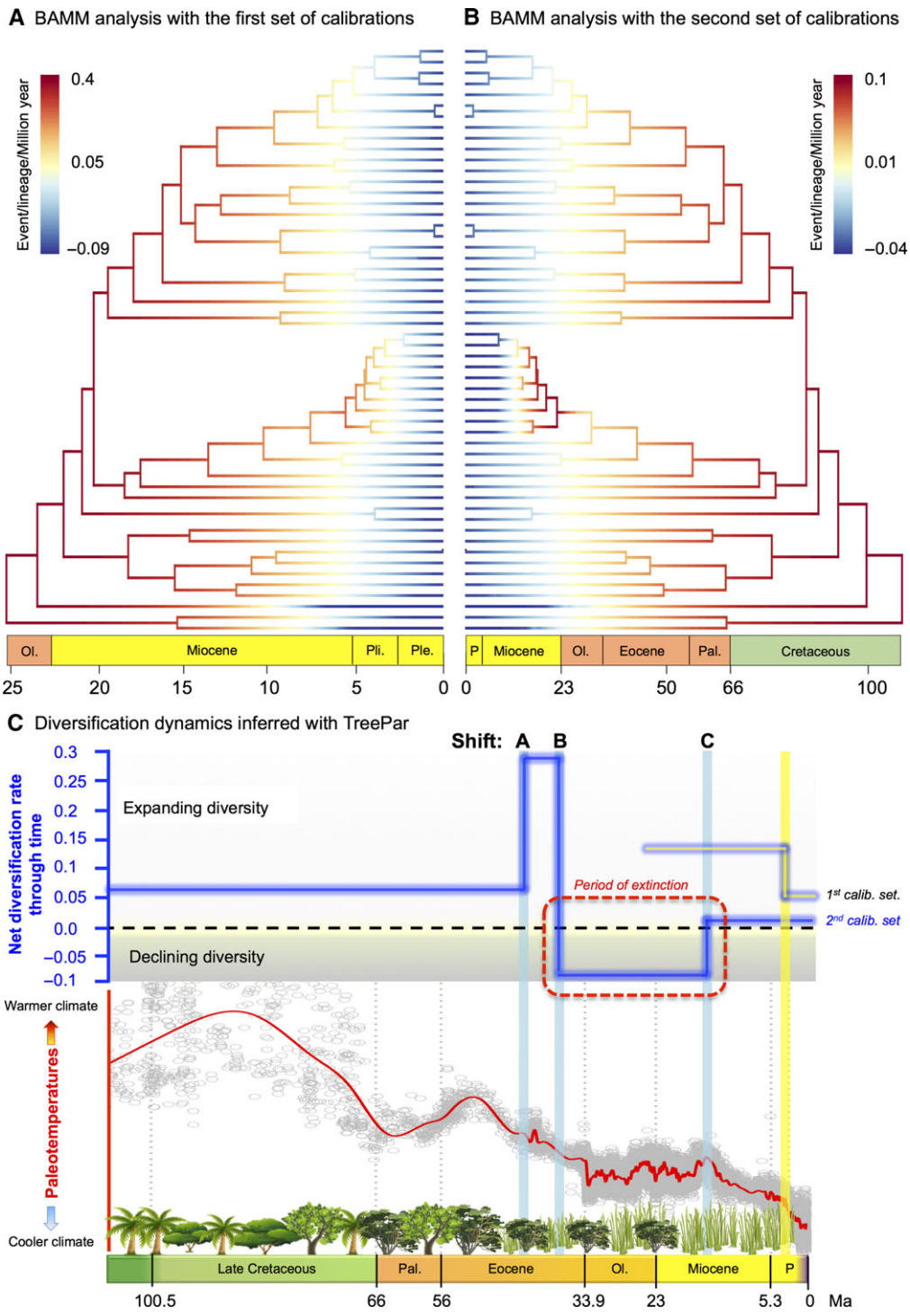

Figure 4. Estimates of the net diversification rates along the burying beetles phylogeny inferred from BAMM analyses. (A) first calibration set; (B) second calibration set (B). Colours at each point in time along branches denote instantaneous rates of diversification inferred as the mean scenario, with colours indicating mean rates across all the shift configurations sampled in the Bayesian posterior. The inferences with TreePar (C) show the dynamic diversification pattern during the Cenozoic with major shifts of diversification in the late Eocene and the mid-Miocene for the second calibration set: there was a decline of diversity between the late Eocene and the mid-Miocene. Instead a single shift in the late Pliocene is found for the first calibration set. Note that both BAMM and TreePar inferred a decline of diversity within the burying beetles. Pg, Paleogene. The global temperatures profile is from Zachos *et al.* (2001).

Table 3. Results of the diversity-dependence diversification analyses made with DDD

Model	NP	logL	*P* (LRT)	λ	μ	*K*
(a) Timetree obtained with the first calibration scenario						
DDL	**2**	**−167.1323**	**Null model**	**0.2064**	–	**85.87**
DDL+E	3	−166.7508	0.382	0.3256	0.05846	69.97
DDX+E	3	−166.6264	0.314	0.7299	0.00043	683579.32
DD+EL	3	−171.7971	0.99	0.1107	≈0	Inf
DD+EX	3	−170.187	0.99	0.149	≈ 0	72.27
(b) Timetree obtained with the second calibration scenario						
DDL	**2**	**−242.0015**	**Null model**	**0.0478**	–	**88.27**
DDL+E	3	−241.5037	0.318	0.081	0.01604	69.33
DDX+E	3	−241.5087	0.321	0.1563	0.00015	657325.71
DD+EL	3	−246.1536	0.99	0.0266	≈ 0	11375.11
DD+EX	3	−246.955	0.99	0.0295	0.00404	Inf

The five diversity-dependence models are described as follows: DDl, speciation declines linearly with diversity and no extinction; DDL+E, speciation declines linearly with diversity and extinction; DDX+E, speciation declines exponentially with diversity and extinction; DD+EL, extinction increases linearly with diversity; and DD+EX, extinction increases exponentially with diversity. Abbreviations are as follows: NP, number of parameters; logL, log-likelihood; *P* (LRT), *P*-value for the likelihood ratio test; λ, estimate of the speciation rate; μ, estimate of the extinction rate; and K, estimate of the carrying capacity of the clade. Bold values depict the best-fit diversification model.

MCC tree, except the third one (Table S2). More importantly we also inferred a pattern of diversity decline in the mid-Cenozoic.

The BAMM analyses converged well as indicated by the stationarity of the MCMC and ESS values above 200 (Fig. S3, S4). Both posterior probabilities and Bayes factors supported a diversification pattern with no clade-specific shift of diversification, and for both timetrees (Figs S5 and S6). More specifically, the post burn-in posterior distribution (901 trees) of the number of shifts indicated for each calibration set that 464/636 trees supported zero shift (PP = 0.52/0.71), 331/220 trees supported one shift (PP = 0.37/0.24), 87/44 trees supported two shifts (PP = 0.097/0.049), 17/1 trees supported three shifts (PP = 0.019/0.001), and 2/0 supported four shifts (PP = 0.002). The BAMM analyses indicated that rates of diversification decreased through time, with higher rates of diversification at the origin of the clade and lower rates towards the Present (Fig. 4). Interestingly, the net diversification rates of *Nicrophorus* turned out to be negative around 3 Mya and 15 Mya, for the first and second calibration set respectively (Fig. 4). The negative diversification rate is indicative of a period of diversity declines (i.e. species loss). These changes are congruent with the first shift time inferred with TreePar. The distinct shift configurations in the credible set (with the highest posterior probabilities) are provided in Figure S7 and Figure S8, and the best configuration shift is depicted in Figure S9 and Figure S10.

The DDD analyses indicated that the best-fitting model for both timetrees is the one in which speciation declines linearly with diversity without extinction (all *P* (LRT) > 0.05 for more complex models, Table 3). The DDD analyses further showed that the clade has not reached a potential carrying capacity as indicated by the estimates of K that are not equal or close to the current species diversity of the clade for both timetrees: the clade has reached 75% and 73%, respectively, of its estimated ecological carrying capacity.

DISCUSSION

Diversification history of burying beetles

Our study suggests that burying beetles likely originated at the end of the Early Cretaceous in the East Palearctic, which at that time was an isolated continent separated from West Palearctic (by the Turgai Sea) and from Africa and India (by the Tethys Sea) (Seton *et al.*, 2012). These results are in agreement with the recent fossil record of the genus discovered in Myanmar (Late Cretaceous, Cenomanian, ~ 93.9–100.5 Mya; Cai *et al.*, 2014). The group diversified in East Palearctic during the Cretaceous without expanding to neighbouring regions, except a single dispersal event towards Southeast Asia (*N. distinctus* occurs in Sulawesi). The Cretaceous is known for its warm and homogeneous climate, in part due to the Tethys Sea connecting the tropical oceans east to

west that helped in warming the global climate (Chaboureau *et al.*, 2014). Warm-adapted groups are known from localities as far as Alaska and Greenland (e.g. palms, Couvreur, Forest & Baker, 2011) or as Antarctica and Patagonia (e.g. cycads, Cúneo *et al.*, 2010), while non-avian dinosaur fossils have been mostly found in Northern Laurasia especially North America and China (Brusatte *et al.*, 2015). It is thus likely that ancestral burying beetles were a warm-adapted group, potentially living in a subtropical (or tropical) region. The diversification analyses indicate the diversification was steady during the Cretaceous, suggesting that the East Palearctic was an 'evolutionary cradle and museum of diversity' for this group, a pattern also recovered in mammals (Tamm & Ramakrishnan, 2015).

At the K-Pg boundary, three independent and simultaneous dispersal events towards Nearctic occurred. Our divergence time estimates suggest these dispersals may have been possible through the Beringia Land Bridge or the De Geer (Thulean) route (Brikiatis, 2014). Our biogeographic analyses support the role of the Beringia Land Bridge as the main dispersal route for burying beetles since we only recover dispersal from East Palearctic to Nearctic (the group did not expand to the West Palearctic, probably because the Turgai Sea was a strong physical barrier for dispersal). Our results are in line with paleogeographic reconstructions suggesting a *terra firma* connection between North America and East Palearctic (Condamine, Sperling & Kergoat, 2013; Brikiatis, 2014). Given the warm climate conditions that lasted from the Cretaceous to the mid-Eocene (Zachos *et al.*, 2001), the dispersal in such elevated latitudes may have been possible (a pattern also recovered in other groups, e.g. Couvreur *et al.*, 2011).

East Palearctic has been a pivotal biogeographic crossroads for the evolution of the burying beetles. We infer that the clade colonized almost all newly adjacent areas in the mid-Paleogene, notably with several expansions towards the West Palearctic and the Oriental region. These colonizations are synchronous with a burst of species formation (shift A in Fig. 4), associated with a three-fold increase of the rate of diversification in the late Eocene (between 41 and 37 Mya). This increase of species accumulation may tentatively be interpreted as the result of the invasions of new geographic regions, especially in areas where potentially no insect group displayed the ecological roles and functions of burying beetles.

One of the most interesting results we infer is a shift of diversification occurring in the late Eocene (37 Mya) when extinction rate was higher than speciation rate, resulting in a drastic loss of species (shift B in Fig. 4). We also estimated that this extinction period lasted *ca.* 20 Myr, until the diversification dynamics of the clade changed again in the mid-Miocene (16 Mya, shift C in Fig. 4). The ensuing question 'what explains such a long and important decline of diversity?' is complex. Here we put forward some hypotheses such as a direct and physical factor inducing an abrupt change in diversification like climate change. The hypothesis of climate change seems likely given the important cooling event that occurred at the late Oligocene, 33.9 Mya (Liu *et al.*, 2009). This change from a warm to a cool climate is thought to have extirpated many species and drove entire clades to extinction at a global scale (e.g. Pearson *et al.*, 2008). Under the assumption that burying beetles were originally a warm-adapted clade, such a sudden and strong cooling event might have had a dramatic impact on the group's diversity. An alternative explanation may be the faunistic turnover induced by the Cenozoic climate change, which was especially marked in the tetrapods (Figueirido *et al.*, 2012; Quental & Marshall, 2013). Burying beetles are mostly associated with small tetrapods (birds and rodents), which have experienced significant extinction periods in the Oligocene and Miocene (some went extinct during this interval) like the Eomyidae, Gliridae, Herpetotheriidae, Nyctitheriidae, Ochotonidae, Omomyidae; all of them occurred in Eurasia and North America (Quental & Marshall, 2013), and were potential hosts for burying beetles. Under this scenario, burying beetles might have suffered from a domino-effect where the extinction of the fauna they depend upon would have fostered their wane (Brodie *et al.*, 2014). In any case, this extinction period likely accounts for the phylogenetic tree shape (long branches) and the relatively low current diversity of the group (68 species), given that the clade appeared 109 Mya.

Inferring extinction using phylogenies is a novel field (Morlon, 2014), and there is much debate to know if it is possible or not to accurately estimate extinction with phylogenies only. We do not deny that estimating extinction rates from reconstructed phylogenies is notoriously difficult (Quental & Marshall, 2010), but papers have contradicted the widespread idea that extinction rates cannot be estimated from molecular phylogenies (Morlon, Parsons & Plotkin, 2011; Beaulieu & O'Meara, 2015). Biases in estimates of extinction rates often come from fitting models based on underlying hypotheses that are violated in nature, such as fitting models with homogeneous rates across clades when major rate shifts occurred (see Morlon *et al.*, 2011; but see Beaulieu & O'Meara, 2015). Our approaches should in principle help with these issues, because BAMM explicitly accounts for rate heterogeneity across clades while allowing rates to vary over time (Rabosky *et al.*, 2013; Rabosky, 2014). Nonetheless, to get more confidence in the macroevolutionary inferences, we

recommend as best practice the use of multiple trees to infer diversification dynamics. The use of posterior trees seem particularly relevant for TreePar analyses that are sensitive to dating uncertainties when using a fine-scale temporal grid (like here grid = 0.1 Myr). Doing so we demonstrated that the extinction pattern inferred with TreePar is robust to dating uncertainties (Table S2). Said that, We also share Beaulieu & O'Meara (2015)'s view that we should remain prudent about estimating extinction from molecular phylogenies. Interestingly, our results are not isolated since other phylogenetic studies have evidenced extinction periods in insect clades (Condamine & Hines, 2015; Toussaint *et al.*, 2015).

While the Neogene is an icehouse period, we infer a last change in diversification dynamics (shift C in Fig. 4) in the mid-Miocene from a pattern of declining diversity to a pattern of expanding diversity (although with low diversification rates). It is thus possible that, while the extreme cooling event at the Eocene-Oligocene boundary pushed the clade to higher extinction rates, the climatic changes may have acted as a species selection within the group, and later triggered pulses of diversification among surviving lineages. At the same time, this change of diversification regime is associated with another wave of biogeographic colonizations, notably in the Neotropics through the Panama Land Bridge in the mid-Miocene (Montes *et al.*, 2015). We also evidence an important phase of species diversification for a subclade that spread into the Oriental and Australasian regions, a range expansion made possible by the tectonic collision of these two regions in the early to mid-Miocene (Hall, 2012, 2013).

Impact of the fossil record on macroevolutionary inferences

Our results highlight major discrepancies between the two sets of calibrations used to obtain absolute divergence time estimates (Figs 2 and 3). The implementation of different prior distributions to inform fossil calibrations did not allow obtaining comparable age estimates between the two calibration sets (Fig. 2, Fig. S2). The analyses based on the first set of calibrations recover an origin of the genus *Nicrophorus* in the late Paleogene, whereas the analyses based on the second set of calibrations find an origin of the group in the mid-Cretaceous as suggested by Sikes & Venables (2013). This represents a difference of more than 60 Myr at the root of the clade that had deep consequences on the inference of macroevolutionary patterns on one hand and the interpretation of the latter on the other hand.

The biogeographic analyses surprisingly recover an identical pattern of geographic range evolution for both chronograms, while taking into account the paleogeographic history (Fig. 3). This is likely due to the fact that the genus *Nicrophorus* is mainly a continental radiation and therefore the modifications of the adjacency matrix or dispersal rate probabilities are less critical than in insular settings (e.g. Ree & Smith, 2008). Although the ancestral ranges inferred are similar, the interpretation of these results differs greatly as the corresponding timescales are markedly different. Three major biogeographic discrepancies can be highlighted:

1. Both reconstructions recover an origin of the genus in East Palearctic followed by broadly simultaneous dispersal events toward the Nearctic region. However, in the first calibration set, the MMCO (Fig. 3) can be invoked to explain these dispersal events. Although in both cases a Beringian land bridge can be implied (Brikiatis, 2014) the causality of the dispersal that can be invoked are radically different.
2. Similarly the colonization of Australasia out of the Oriental region is interpreted differently in the first calibration set. This colonization is suggested to have happened in the past 5 Myr. This period is marked by Plio-Pleistocene glaciations that have shaped the fate of clades in the Indo-malayan-Australasian archipelago due to sea-level fluctuations and/or climatic disruptions (Toussaint *et al.*, 2013). In contrast, the second set of calibrations implies a colonization during the early Miocene when both the Sunda and Sahul regions collided (Seton *et al.*, 2012). This geological rearrangement resulted in a massive orogeny in Wallacea (Hall, 2012, 2013) and Melanesia (Toussaint *et al.*, 2014) responsible for the exchange of biotas between the Oriental and Australian regions (Tänzler *et al.*, 2014; Toussaint *et al.*, 2014; Condamine *et al.*, 2015). Hence, these contrasting results imply either a climatic or a geological factor to explain the biogeographic history of *Nicrophorus* in Southeast Asia.
3. The biogeographic reconstruction based on the first calibration set recovers four Neotropical colonization events in the last 4 Myr (Fig. 3). The colonization of the Neotropics is tightly linked to the emergence of the Panama Isthmus (e.g. Great American Biotic Interchange, Webb, 2006). Our results exemplify well the long-standing debate between a late Pliocene (3.5 Mya) vs. a mid-Miocene ($\approx$ 15 Mya) origin of the closure of the Central American Seaway (Cody *et al.*, 2010). This geological structure is pivotal for the understanding of the New World biotic evolution, and our second calibration set is in agreement with the latest geological evidence (Montes *et al.*, 2015).

A similar discussion can be drawn with the analyses of the diversification rates. Both trees evidence an interesting pattern of extinction with BAMM. Both trees also show a pattern with higher diversification rates in the early stage of the group's evolution and a subsequent slowdown of the diversification toward the Present (Fig. 4a). The main difference in the BAMM analyses is the pace at which the clade diversified. Clearly this difference can only be attributed to the different ages obtained with the two calibration sets. Interestingly the TreePar analyses are markedly incongruent between the two dating analyses. TreePar only found a single (supported) shift of diversification in the Pliocene for the first calibration set, but found a more dynamic diversification history for the second set of calibrations with three significant changes of diversification (Fig. 4b). In the latter, TreePar identified a period of extinction (see above for a discussion), which is not inferred with the first calibration set, and is robust to dating uncertainties (Table S2).

Altogether, these results highlight the impact the fossil record can have on the macroevolutionary inferences of a focal clade. We do not think these results are trivial given the fossil record of carrion and burying beetles, but instead think that the situation represented by the first calibration set is more common than previously thought, especially in invertebrate clades for which the fossil record is poorly documented and studied. Novel discoveries, probably in ancient (Jurassic and Cretaceous) fossil deposits such as in China, may well reveal a very different evolutionary history for several clades.

CONCLUSION

Our study suggests that best practices in the treatment of fossil data using Bayesian relaxed-clock and three prior distributions on fossil calibration may not be sufficient to acknowledge the possible lack of fossils in some groups. We show that even a thorough comparison of molecular dating analytical settings cannot solely alleviate the taphonomic bias, at least in silphids. Analyses of additional clades as well as simulation studies will be valuable to understand the detailed effects of taphonomic biases on age estimates. Divergence time estimates critically depend upon the completeness of available fossil records. Further paleontological research is needed to speed up insect fossil discoveries especially in Jurassic and Cretaceous Chinese fossil beds.

ACKNOWLEDGEMENTS

Two anonymous reviewers are acknowledged for constructive comments on earlier versions of this article. We particularly wish to thank Derek Sikes and Chandra Venables for making their molecular dataset available. Gael J. Kergoat is acknowledged for helpful comments. Finally, we would like to warmly thank Alfred Newton and Chenyang Cai for fruitful discussions regarding the fossil record of carrion beetles.

REFERENCES

Alroy J. 2010. The shifting balance of diversity among major marine animal groups. *Science* **329:** 1191–1194.

Beaulieu JM, O'Meara BC. 2015. Extinction can be estimated from moderately sized molecular phylogenies. *Evolution* **69:** 1036–1043.

Bell CD. 2015. Between a rock and a hard place: Applications of the "molecular clock" in systematic biology. *Systematic Botany* **40:** 6–13.

Beutel RG, Leschen RAB. 2005. *Handbook of Zoology, Vol. IV Arthropoda: Insecta, Part 38, Evolution and Systematics Coleoptera (Archostemata, Adephaga, Myxophaga, Polyphaga part)*. Waltyer de Gruyter, Berlin.

Blakey RC. 2008. Gondwana paleogeography from assembly to breakup – a 500 million year odyssey. In: CR Fielding, TD Frank, IsbellJ L, eds. *Resolving the late Paleozoic ice age in time and space*, Boulder (CO): Geological Society of America Special Paper 441, 1–28.

Brikiatis L. 2014. The De Geer, Thulean and Beringia routes: key concepts for understanding early Cenozoic biogeography. *Journal of Biogeography* **41:** 1036–1054.

Brodie JF, Aslan CE, Rogers HS, Redford KH, Maron JL, Bronstein JL, Groves CR. 2014. Secondary extinctions of biodiversity. *Trends in Ecology and Evolution* **29:** 664–672.

Brusatte SL, Butler RJ, Barrett PM, Carrano MT, Evans DC, Lloyd GT, Mannion PD, Norell MA, Peppe DJ, Upchurch P, Williamson TE. 2015. The extinction of the dinosaurs. *Biological Reviews* **90:** 628–642.

Cai CY, Thayer MK, Engel MS, Newton AF, Ortega-Blanco J, Wang B, Wang X-D, Huang D-Y. 2014. Early origin of parental care in Mesozoic carrion beetles. *Proceeding of the National Academy of Sciences USA* **111:** 14170–14714.

Chaboureau AC, Sepulchre P, Donnadieu Y, Franc A. 2014. Tectonic-driven climate change and the diversification of angiosperms. *Proceeding of the National Academy of Sciences USA* **111:** 14066–14070.

Chang SC, Zhang H, Renne PR, Fang Y. 2009. High-precision $^{40}Ar/^{39}Ar$ age for the Jehol Biota. *Palaeogeography Palaeoclimatology Palaeoecology* **280:** 94–104.

Choiniere JN, Xu X, Clark JM, Forster CA, Guo Y, Han FA. 2010. A basal alvarezsauroid theropod from the early Late Jurassic of Xinjiang, China. *Science* **327:** 571–574.

Cody S, Richardson JE, Rull V, Ellis C, Pennington RT. 2010. The Great American Biotic Interchange revisited. *Ecography* **33:** 326–332.

Condamine FL, Hines HM. 2015. Historical species losses in bumblebee evolution. *Biology Letters* **11:** 20141049.

Condamine FL, Sperling FAH, Kergoat GJ. 2013. Global biogeographical pattern of swallowtail diversification demonstrates alternative colonization routes in the Northern and Southern hemispheres. *Journal of Biogeography* **40:** 9–23.

Condamine FL, Toussaint EFA, Clamens AL, Genson G, Sperling FAH, Kergoat GJ. 2015. Deciphering the evolution of birdwing butterflies 150 years after Alfred Russel Wallace. *Scientific Reports* **5:** 11680.

Couvreur TLP, Forest F, Baker W. 2011. Origin and global diversification patterns of tropical rain forests: inferences from a complete genus-level phylogeny of palms. *BMC Biology* **9:** 44.

Cúneo NR, Escapa I, Villar de Seoane L, Artabe A, Gnaedinger S 2010. Review of the Cycads and Bennettitaleans from the Mesozoic of Argentina. In: Gee CT ed. *Plants in mesozoic time: morphological innovations, phylogeny, ecosystems*, Bloomington: Indiana University Press, 187–212.

Donoghue PCJ, Benton MJ. 2007. Rocks and clocks: calibrating the Tree of Life using fossils and molecules. *Trends in Ecology and Evolution* **22:** 424–431.

Dornburg A, Beaulieu JM, Oliver JC, Near TJ. 2011. Integrating fossil preservation biases in the selection of calibrations for molecular divergence time estimation. *Systematic Biology* **60:** 519–527.

Drummond AJ, Ho SYW, Phillips MJ, Rambaut A. 2006. Relaxed phylogenetics and dating with confidence. *PLoS Biology* **4:** 699–710.

Drummond AJ, Suchard MA, Xie D, Rambaut A. 2012. Bayesian phylogenetics with BEAUti and the BEAST 1.7. *Molecular Biology and Evolution* **29:** 1969–1973.

Etienne RS, Haegeman B, Stadler T, Aze T, Pearson PN, Purvis A, Philimore AB. 2012. Diversity-dependence brings molecular phylogenies closer to agreement with the fossil record. *Proceedings of the Royal Society of London B* **279:** 1300–1309.

Figueirido B, Janis CM, Pérez-Claros JA, De Renzi M, Palmqvist P. 2012. Cenozoic climate change influences mammalian evolutionary dynamics. *Proceeding of the National Academy of Sciences USA* **109:** 722–727.

Flach C. 1890. Ueber zwei fossile Silphiden (Coleoptera) aus den Phosphoriten von Caylux. *Deutsche Entomologische Zeitschrift* **1:** 105–109.

Gao K-Q, Shubin NH. 2003. Earliest known crown-group salamanders. *Nature* **422:** 424–428.

Gao K-Q, Shubin NH. 2012. Late Jurassic salamandroid from western Liaoning, China. *Proceeding of the National Academy of Sciences USA* **109:** 5767–5772.

Garrouste R, Clément G, Nel P, Engel MS, Grandcolas P, D'Haese C, Lagebro L, Denayer J, Gueriau P, Lafaite P, Olive S, Prestianni C, Nel A. 2012. A complete insect from the Late Devonian period. *Nature* **488:** 82–85.

Gernhard T. 2008. The conditioned reconstructed process. *Journal of Theoretical Biology.* **253:** 769–778.

Grebennikov VV, Newton AF. 2012. Detecting the basal dichotomies in the monophylum of carrion and rove beetles (Insecta: Coleoptera: Silphidae and Staphylinidae) with emphasis on the Oxyteline group of subfamilies. *Arthropod Systematics and Phylogeny* **70:** 133–165.

Hall R. 2012. Late Jurassic-Cenozoic reconstructions of the Indonesian region and the Indian Ocean. *Tectonophysics* **570:** 1–41.

Hall R. 2013. The palaeogeography of Sundaland and Wallacea since the Late Jurassic. *Journal of Limnology* **72:** 1–17.

Hedges SB, Kumar S. 2009. *The timetree of life*. Oxford: Oxford University Press.

Hedges SB, Marin J, Suleski M, Paymer M, Kumar S. 2015. Tree of life reveals clock-like speciation and diversification. *Molecular Biology and Evolution* **32:** 835–845.

Ho SYW, Duchêne D. 2014. Molecular-clock methods for estimating evolutionary rates and timescales. *Molecular Ecology* **23:** 5947–5965.

Ho SYW, Phillips MJ. 2009. Accounting for calibration uncertainty in phylogenetic estimation of evolutionary divergence times. *Systematic Biology* **58:** 367–380.

Hu D, Hou L, Zhang L, Xu X. 2009. A pre-Archaeopteryx troodontid theropod from China with long feathers on the metatarsus. *Nature* **461:** 640–643.

Huang D, Engel MS, Cai C, Wu H, Nel A. 2012. Diverse transitional giant fleas from the Mesozoic era of China. *Nature* **483:** 201–204.

Huang D, Nel A, Cai C, Lin Q, Engel MS. 2013. Amphibious flies and paedomorphism in the Jurassic period. *Nature* **495:** 94–97.

Huelsenbeck JP, Larget B, Alfaro ME. 2004. Bayesian phylogenetic model selection using reversible jump Markov chain Monte Carlo. *Molecular Biology and Evolution* **21:** 1123–1133.

Inoue J, Donoghue PCJ, Yang Z. 2010. The impact of the representation of fossil calibrations on Bayesian estimation of species divergence times. *Systematic Biology* **59:** 74–89.

Kass RE, Rafferty AE. 1995. Bayes factors. *Journal of the American Statistical Association* **90:** 773–795.

Kirejtshuk AG, Ponomarenko AG, Prokin AA, Chang HL, Nikolajev GV, Ren D. 2010. Current knowledge of Mesozoic Coleoptera from Daohugou and Liaoning (Northeast China). *Acta Geologica Sinica* **84:** 783–792.

Kodandaramaiah U. 2011. Tectonic calibrations in molecular dating. *Current Zoology* **57:** 116–124.

Lanfear R, Calcott B, Ho SYW, Guindon S. 2012. PartitionFinder: combined selection of partitioning schemes and substitution models for phylogenetic analyses. *Molecular Biology and Evolution* **29:** 695–1701.

Lee MS, Cau A, Naish D, Dyke GJ. 2014. Morphological clocks in paleontology, and a mid-Cretaceous origin of crown Aves. *Systematic Biology* **63:** 442–449.

Liu Z, Pagani M, Zinniker D, DeConto R, Huber M, Brinkhuis H, Shah SR, Leckie RM, Pearson A. 2009. Global cooling during the Eocene-Oligocene climate transition. *Science* **323:** 1187–1190.

Lu PJ, Yogo M, Marshall CR. 2006. Phanerozoic marine biodiversity dynamics in light of the incompleteness of the fossil record. *Proceeding of the National Academy of Sciences USA* **103:** 2736–2739.

Lukoschek V, Scott Keogh J, Avise JC. 2012. Evaluating fossil calibrations for dating phylogenies in light of rates of molecular evolution: a comparison of three approaches. *Systematic Biology* **61:** 22–43.

Luo Z-X. 2007. Transformation and diversification in early mammal evolution. *Nature* **450:** 1011–1019.

McVay JD, Flores-Villela O, Carstens B. 2015. Diversification of North American natricine snakes. *Biological Journal of the Linnean Society* **116:** 1–12.

Meng Q-J, Ji Q, Zhang Y-G, Liu D, Grossnickle DM, Luo Z-X. 2015. An arboreal docodont from the Jurassic and mammaliaform ecological diversification. *Science* **347:** 764–768.

Montes C, Cardona A, Jaramillo C, Pardo A, Silva JC, Valencia V, Ayala C, Pérez-Angel LC, Rodriguez-Parra LA, Ramirez V, Niño H. 2015. Middle Miocene closure of the Central American Seaway. *Science* **348:** 226–229.

Morlon H. 2014. Phylogenetic approaches for studying diversification. *Ecology Letters* **17:** 508–525.

Morlon H, Parsons TL, Plotkin JB. 2011. Reconciling molecular phylogenies with the fossil record. *Proceeding of the National Academy of Sciences USA* **108:** 16327–16332.

Nel A, Roques P, Nel P, Prokin AA, Bourgoin T, Prokop J, Szwedo J, Azar D, Desutter-Grandcolas L, Wappler T, Garrouste R, Coty D, Huang D, Engel MS, Kirejtshuk G. 2013. The earliest known holometabolous insects. *Nature* **503:** 257–261.

Newton AF. 1997. Review of Agyrtidae (Coleoptera), with a new genus and species from New Zealand. *Annales Zoologici Fennici* **47:** 111–156.

Parham JF, Donoghue PCJ, Bell CJ, Calway TD, Head JJ, Holroyd PA, Inoue JG, Irmis RB, Joyce WG, Ksepka DT, Patané JSL, Smith ND, Tarver JE, van Tuinen M, Yang Z, Angielczyk KD, Greenwood JM, Hipsley CA, Jacobs L, Makovicky PJ, Müller J, Smith KT, Theodor JM, Warnock RCM. 2012. Best practices for justifying fossil calibrations. *Systematic Biology* **61:** 346–359.

Pearson PN, McMillan IK, Wade BS, Dunkley Jones T, Coxall HK, Bown PR, Lear CH. 2008. Extinction and environmental change across the Eocene-Oligocene boundary in Tanzania. *Geology* **36:** 179–182.

Peña C, Witthauer H, Kleckova I, Fric Z, Wahlberg N. 2015. Adaptive radiations in butterflies: evolutionary history of the genus *Erebia* (Nymphalidae: Satyrinae). *Biological Journal of the Linnean Society* **116:** 449–467.

Quental TB, Marshall CR. 2010. Diversity dynamics: molecular phylogenies need the fossil record. *Trends in Ecology and Evolution* **25:** 434–441.

Quental TB, Marshall CR. 2013. How the Red Queen drives terrestrial mammals to extinction. *Science* **341:** 290–292.

Rabosky DL. 2014. Automatic detection of key innovations, rate shifts, and diversity dependence on phylogenetic trees. *PLoS ONE* **9:** e89543.

Rabosky DL, Santini F, Eastman JM, Smith SA, Sidlauskas B, Chang J, Alfaro ME. 2013. Rates of speciation and morphological evolution are correlated across the largest vertebrate radiation. *Nature Communications* **4:** 1958.

Rabosky DL, Grundler M, Anderson C, Title P, Shi JJ, Brown JW, Huang H, Larson JG. 2014. BAMMtools: an R package for the analysis of evolutionary dynamics on phylogenetic trees. *Methods in Ecology and Evolution* **5:** 701–707.

Rainford JL, Hofreiter M, Nicholson DB, Mayhew PJ. 2014. Phylogenetic distribution of extant richness suggests metamorphosis is a key innovation driving diversification in insects. *PLoS ONE* **9:** e109085.

Rambaut A, Suchard MA, Xie W, Drummond AJ. 2015. Tracer v1.6. Available: http://tree.bio.ed.ac.uk/software/tracer.

Ree RH, Smith SA. 2008. Maximum likelihood inference of geographic range evolution by dispersal, local extinction, and cladogenesis. *Systematic Biology* **57:** 4–14.

Ronquist F, Teslenko M, Van der Mark P, Ayres DL, Darling A, Höhna S, Larget B, Liu L, Suchard MA, Huelsenbeck JP. 2012. MrBayes 3.2: efficient Bayesian phylogenetic inference and model choice across a large model space. *Systematic Biology* **61:** 539–542.

Rutschmann F. 2006. Molecular dating of phylogenetic trees: a brief review of current methods that estimate divergence times. *Diversity and Distributions* **12:** 35–48.

Sanders KL, Lee MS. 2007. Evaluating molecular clock calibrations using Bayesian analyses with soft and hard bounds. *Biology Letters* **3:** 275–279.

Selden PA, Shih C, Ren D. 2011. A golden orb-weaver spider (Araneae: Nephilidae: *Nephila*) from the Middle Jurassic of China. *Biology Letters* **7:** 775–778.

Seton M, Müller RD, Zahirovic S, Gaina C, Torsvik T, Shephard G, Talsma M, Gurnis M, Turner M, Maus S, Chandler M. 2012. Global continental and ocean basin reconstructions since 200 Ma. *Earth Science Reviews* **113:** 212–270.

Sikes DS, Venables C. 2013. Molecular phylogeny of the burying beetles (Coleoptera: Silphidae: Nicrophorinae). *Molecular Phylogenetics and Evolution* **69:** 552–565.

Sikes DS, Madge RB, Newton AF. 2002. A catalog of the Nicrophorinae (Coleoptera: Silphidae) of the world. *Zootaxa* **65:** 1–304.

Sikes DS, Madge RB, Trumbo ST. 2006. Revision of *Nicrophorus* in part: new species and inferred phylogeny of the *nepalensis* group based on evidence from morphology and mitochondrial DNA (Coleoptera: Silphidae: Nicrophorinae). *Invertebrate Systematics* **20:** 305–365.

Smith DM, Marcot JD. 2015. The fossil record and macroevolutionary history of the beetles. *Proceedings of the Royal Society of London B* **282:** 20150060.

Smith AB, Peterson KJ. 2002. Dating the time of origin of major clades: molecular clocks and the fossil record. *Annual Review of Ecology, Evolution and Systematics* **30:** 65–88.

Sohn J-C, Labandeira CC, Davis DR. 2015. The fossil record and taphonomy of butterflies and moths (Insecta, Lepidoptera): implications for evolutionary diversity and divergence-time estimates. *BMC Evolutionary Biology* **15:** 12.

Stadler T. 2011. Mammalian phylogeny reveals recent diversification rate shifts. *Proceeding of the National Academy of Sciences USA* **108:** 6187–6192.

Su YC, Chang YH, Smith D, Zhu MS, Kuntner M, Tso IM. 2011. Biogeography and speciation patterns of the golden orb spider genus *Nephila* (Araneae: Nephilidae) in Asia. *Zoological Science* **28:** 47–55.

Swofford DL 2003. PAUP*. Phylogenetic Analysis Using Parsimony (*and Other Methods). Version 4. Sinauer Associates, Sunderland, Massachusetts.

Sytsma KJ, Spalink D, Berger B. 2014. Calibrated chronograms, fossils, outgroup relationships, and root priors: re-examining the historical biogeography of Geraniales. *Biological Journal of the Linnean Society* **113:** 29–49.

Tamm K, Ramakrishnan U. 2015. Higher speciation and lower extinction rates influence mammal diversity gradients in Asia. *BMC Evolutionary Biology* **15:** 11.

Tänzler R, Toussaint EFA, Suhardjono YR, Balke M, Riedel A. 2014. Multiple transgressions of Wallace's line explain diversity of flightless *Trigonopterus* weevils on Bali. *Proceedings of the Royal Society of London B* **281:** 20132528.

Toussaint EFA, Sagata K, Surbakti S, Hendrich L, Balke M. 2013. Australasian sky islands act as a diversity pump facilitating peripheral speciation and complex reversal from narrow endemic to widespread ecological supertramp. *Ecology and Evolution* **3:** 1031–1049.

Toussaint EFA, Hall R, Monaghan MT, Sagata K, Ibalim S, Shaverdo HV, Vogler AP, Pons J, Balke M. 2014. The towering orogeny of New Guinea as a trigger for arthropod megadiversity. *Nature Communications* **5:** 4001.

Toussaint EFA, Condamine FL, Hawlitschek O, Watts CH, Porch N, Hendrich L, Balke M. 2015. Unveiling the diversification dynamics of Australasian predaceous diving beetles in the Cenozoic. *Systematic Biology* **64:** 3–24.

Wang X, Zhou Z, He H, Jin F, Wang Y, Zhang J, Wang Y, Xu X, Zhang F. 2005. Stratigraphy and age of the Daohugou bed in Ningcheng, Inner Mongolia. *Chinese Science Bulletin* **50:** 2369–2376.

Warnock RCM, Parham JF, Joyce WG, Lyson TR, Donoghue PCJ. 2015. Calibration uncertainty in molecular dating analyses: there is no substitute for the prior evaluation of time priors. *Proceedings of the Royal Society of London B* **282:** 20141013.

Webb SD. 2006. The great American biotic interchange: patterns and processes. *Annals of the Missouri Botanical Garden* **93:** 245–257.

Xu X, Zheng X, You H. 2010. Exceptional dinosaur fossils show ontogenetic development of early feathers. *Nature* **464:** 1338–1341.

Xu X, You H, Du K, Han F. 2011. An Archaeopteryx-like theropod from China and the origin of Avialae. *Nature* **475:** 465–470.

Xu X, Zheng X, Sullivan C, Wang X, Xing L, Wang Y, Zhang X, O'Connor JK, Zhang F, Pan Y. 2015. A bizarre Jurassic maniraptoran theropod with preserved evidence of membranous wings. *Nature* **521:** 70–73.

Yang Z, Rannala B. 2006. Bayesian estimation of species divergence times under a molecular clock using fossil calibrations with soft bounds. *Molecular Biology and Evolution* **23:** 212–226.

Yuan C-X, Ji Q, Meng Q-J, Tabrum AR, Luo Z-X. 2013. Earliest evolution of Multituberculate mammals revealed by a new Jurassic fossil. *Science* **341:** 779.

Zachos J, Pagani M, Sloan L, Thomas E, Billups K. 2001. Trends, rhythms, and aberrations in global climate 65 Ma to present. *Science* **292:** 686–693.

Zhang F, Zhou Z, Xu X, Wang X, Sullivan C. 2008. A bizarre Jurassic maniraptoran from China with elongate ribbon-like feathers. *Nature* **455:** 1105–1108.

Zhou CF, Wu S, Martin T, Luo Z-X. 2013. A Jurassic mammaliaform and the earliest mammalian evolutionary adaptations. *Nature* **500:** 163–167.

SUPPORTING INFORMATION

Additional Supporting Information may be found online in the supporting information tab for this article:

Figure S1. Parameters of the prior distributions as specified in BEAUti for the Bayesian dating analyses. The first panel (a) shows the prior exponential distributions and respective BEAUti parameters for each calibrated node in the calibration sets I and II. The second panel (b) shows the prior lognormal distributions and respective BEAUti parameters for each calibrated node in the calibration sets I and II.

Figure S2. Time-calibrated trees of silphids (including the burying beetle clade, genus *Nicrophorus*) for the two calibration sets indicating the 95% credibility intervals for each node. The two-first are obtained with the exponential prior, the two following with the lognormal prior, and the two last with the uniform prior.

Figure S3. Convergence of the BAMM analysis with the chronogram reconstructed with the *first* calibration set. (a) The stationary of the MCMC before applying a burn-in. (b) The posterior distribution of number of shifts estimated before applying a burn-in. (c) The stationary of the MCMC after removing the burn-in phase. (d) The posterior distribution of number of shifts estimated after removing the burn-in phase.

Figure S4. Convergence of the BAMM analysis with the chronogram reconstructed with the *second* calibration set. (a) The stationary of the MCMC before applying a burn-in. (b) The posterior distribution of number of shifts estimated before applying a burn-in. (c) The stationary of the MCMC after removing the burn-in phase. (d) The posterior distribution of number of shifts estimated after removing the burn-in phase.

Figure S5. Frequency distribution of distinct macroevolutionary rate regimes estimated using BAMM and the tree reconstructed with the *first* calibration set. (a) Prior distribution of the number of distinct processes. (b) Posterior distribution of the number of distinct processes (including the root process) for the burying beetles phylogeny.
Figure S6. Frequency distribution of distinct macroevolutionary rate regimes estimated using BAMM and the tree reconstructed with *second* first calibration set. (a) Prior distribution of the number of distinct processes. (b) Posterior distribution of the number of distinct processes (including the root process) for the burying beetles phylogeny.
Figure S7. Credible set of configuration shifts of burying beetles inferred with BAMM using the tree obtained with the *first* calibration set. Phylogenies show the distinct shift configurations with the highest posterior probability. For each shift configuration, the locations of rate shifts are shown as red (rate increases) and blue (rate decreases) circles, with circle size proportional to the marginal probability of the shift. Text labels (e.g. $f = 0.84$ for the first) denote the posterior probability of each shift configuration.
Figure S8. Credible set of configuration shifts of burying beetles inferred with BAMM using the tree obtained with the *second* calibration set. Phylogenies show the distinct shift configurations with the highest posterior probability. For each shift configuration, the locations of rate shifts are shown as red (rate increases) and blue (rate decreases) circles, with circle size proportional to the marginal probability of the shift. Text labels (e.g. $f = 0.86$ for the first) denote the posterior probability of each shift configuration.
Figure S9. The best shift configuration inferred with BAMM using the tree with the *first* calibration set.
Figure S10. The best shift configuration inferred with BAMM using the tree with the *second* calibration set.
Table S1. Matrices of time slices and dispersal rates (a) and the adjacency matrix (b) used for the biogeographic analyses. Abbreviations are as follows: AU, Australasian region (Australia and Sahul Shelf); OR, Oriental region (India and Sunda Shelf); NT, Neotropics (South America, Central America and Caribbean); NE, Nearctic (North America); EP, Eastern Palearctic (Europe); and WP, Western Palearctic (Asia). The rationale of these matrices are explained in the text.
Table S2. Results of the diversification analyses made with TreePar on 100 trees randomly taken in the Bayesian dating analysis of the second set of calibrations. The model with three shifts is supported. Abbreviations are as follows: NP, number of parameters; logL, log-likelihood; *P* (LRT), *P*-value for the likelihood ratio test (LRT are realized sequentially by testing first the null model with the second model; if the second model receives a significant support it becomes the reference for the second LRT against the third model, and so on); r. 1, net diversification rate 1 (from Present to the first shift time going backward); τ 1, turnover 1 (from Present to the first shift time going backward); and s.t. 1, shift time 1 (i.e. period when the diversification changed).